Electrospun SnO$_2$–ZnO nanofibers with improved electrochemical performance as anode materials for lithium-ion batteries

CrossMark

Yang Zhao [a,b], Xifei Li [a,c,], Lei Dong [a], Bo Yan [a], Hui Shan [a], Dejun Li [a,**], Xueliang Sun [a,b,***]*

[a] *Energy & Materials Engineering Centre, College of Physics and Materials Science, Tianjin Normal University, Tianjin 300387, China*
[b] *Nanomaterials and Energy Lab, Department of Mechanical and Materials Engineering, University of Western Ontario, London, Ontario N6A 5B9, Canada*
[c] *Key Laboratory of Advanced Energy Materials Chemistry (Ministry of Education), Collaborative Innovation Center of Chemical Science and Engineering, College of Chemistry, Nankai University, Tianjin 300071, China*

ARTICLE INFO

ABSTRACT

The novel SnO$_2$–ZnO nanofibers were successfully synthesized via a simple electrospinning technique. The influences of different amount of ZnO on the electrochemical properties have been discussed. Compared with SnO$_2$ nanofibers, the SnO$_2$–ZnO nanocomposites show the improved lithium storage capacity, cycling performance and rate properties. The beneficial effects can be attributed to the addition of ZnO nanoparticles, which can effectively buffer the volume exchange of SnO$_2$ and create synergistic effects between them. Thus, as-prepared SnO$_2$–ZnO nanofibers may hold great promise for the development of high-performance lithium ion batteries, and this work can be enlightening for material design and optimization.

Introduction

The global energy shortage strongly demands highly efficient clean energy, such as solar and wind powers, which further require advanced energy conversion and storage devices. As one of the most important energy storage devices, lithium-ion batteries (LIBs) have attracted increasing attention in both scientific and industrial fields as well as people's daily life, such as electric vehicles, cell phones, laptops and digital cameras [1–7]. Although LIBs were developed for many years, they still have not satisfied the application requirements in terms of the energy density, cycle lifetime, and safety [8–12].

The key factor for improving the LIBs performance is to develop better electrode materials [13,14]. Nowadays, the graphite is the most widely employed commercial anode material for LIBs, but its relatively low theoretical capacity (372 mA h g^{-1}) limits further applications [15–18].

As one of the alternative anodes of LIBs, SnO$_2$ has been regarded as a promising candidate due to high theoretical specific capacity of 781 mAh g^{-1} [19–21]. Numerous approaches have been attempted to solve the serious volume changes and internal stress problems of SnO$_2$ anodes. Among the strategies, building unique SnO$_2$ nanostructure is the most effective one, including nanoparticles [22], nanowires [23,24], nanotubes [25,26], nanosheets [27] and 3D nanostructure [28–30]. Furthermore, it has been considered that the low-dimensional nanostructures, such as wires, fibers and tubes, exhibit better buffering effects of volume change [19,23,24]. Another effective approach is to introduce different inorganic nanoparticles to create hybrid nanocomposites to enhance the battery performance, like ZnO [31], In$_2$O$_3$ [32], Fe$_2$O$_3$ [33], TiO$_2$ [34], etc. It was reported that the heterostructures between ZnO and SnO$_2$ provides an enhanced inner electric field at the interface of nanoparticles, moreover, the inactive ZnO can act as a buffering matrix for SnO$_2$ to relief the strain and stress during electrochemical process, which will effectively enhance the performance [31].

The electrospinning is a simple and versatile approach to create fiber-like nanostructures of metal oxides for different applications, including LIBs, photocatalytic activities, gas sensing properties, etc [35–41]. As a result, in this study, the SnO$_2$–ZnO nanofibers were synthesized via the simple electrospinning approach. The hybrid nanocomposites show the improved reversible capacity, cycling performance and rate capability than the pristine fibers. The obvious effects of ZnO nanoparticles in the nanocomposites were discussed in detail. It demonstrates that the as-prepared SnO$_2$–ZnO nanofiber is a promising anode material of LIBs. Our study provides new ideas to build hybrid metal oxide anodes with increased LIB performance.

Experimental section

Materials synthesis

In the typical synthesis of SnO$_2$–ZnO NFs, the precursor solution was prepared by dissolving 1.2 g of PVP (M$_w$ = 1,300,000 g mol^{-1}) and different molar ratio of SnCl$_4$·5H$_2$O and Zn(NO$_3$)$_3$·6H$_2$O in ethyl alcohol (6.6 ml) and DMF (6.6 ml). The mixture was then stirred by vigorous stirring for 24 h at room temperature to form a homogeneous solution.

During electrospinning, a high voltage of 20 kV was applied between the needle tip and aluminum collector. The needle tip to the collector was 15 cm. The flow rate is 1 ml/h. Finally, the as-spun fibers were sintered at 700 °C for 5 h in air. The molar ratio of SnCl$_4$·5H$_2$O and Zn(NO$_3$)$_3$·6H$_2$O was 2:1, 1:1, 1:2, and the resultant samples were marked as SnO$_2$–ZnO-1, SnO$_2$–ZnO-2 and SnO$_2$–ZnO-3, respectively. For comparison, the pristine SnO$_2$ nanofibers were synthesized without the addition of Zn(NO$_3$)$_3$·6H$_2$O, and the syntheses of pristine ZnO was synthesized without the addition of SnCl$_4$·5H$_2$O. The

typical schematic illustration of the formation process ZnO/SnO$_2$ Nanofibers is shown in Scheme 1.

Materials characterization

X-ray diffraction analysis (XRD) (Bruker, D8 Advance) was employed to characterize the structures of the prepared samples. The surface morphologies of the composites were determined using a TEM (JEOL JEM-3000F) and a scanning electron microscope (SEM, SU8010, Hitachi Japan). X-ray photoelectron spectroscopy (XPS, VG ESCALAB MK II) was performed to analyze the distribution of element in the samples.

A battery tester (LAND CT2001A) was used to evaluate the electrochemical performance of CR2032-type coin cells. The working electrodes consisted of samples (75 wt %) and acetylene black (15 wt %), with PVDF (10 wt %) as a binder, dissolved in 1-methyl-2-pyrrolidinone (NMP) solution on a piece of copper foil. Li foil was used as the counter electrode and the reference electrode, and Celgard 2400 was used as a separator. The elecstrolyte was a solution of 1 M LiPF$_6$ in a mixture of ethylene carbonate (EC), dimethyl carbonate (DMC) and diethyl carbonate (DEC) (1: 1: 1, v/v/v). The loading of the typical electrode active material is 1.0 mg cm^{-1}. Cyclic voltammetry (CV) was performed on Princeton Applied Research Versa STAT 4 electrochemical workstation.

Result and discussion

The XRD patterns of the pristine SnO$_2$, the pristine ZnO, SnO$_2$–ZnO-1, SnO$_2$–ZnO-2, and SnO$_2$–ZnO-3 were compared to confirm the component of the products, as shown in Fig. 1a. When the original reactant is SnCl$_4$·5H$_2$O, all the diffraction peaks of the product are in good agreement with the standard SnO$_2$ data (PDF#41-1445). The lattice constants of SnO$_2$ NFs is a = 4.738 Å, b = 4.738 Å, c = 3.187 Å. After the addition of zinc nitrate, the weak peaks positioned at 31.769°, 34.421°, 36.252°, 47.538°, 56.602°, 62.862°, 66.378°, 67.961° and 69.098° correspond to ZnO (PDF#36–1451) with the lattice constants of a = 3.250 Å, b = 3.250 Å, c = 5.207 Å. It illustrates that the
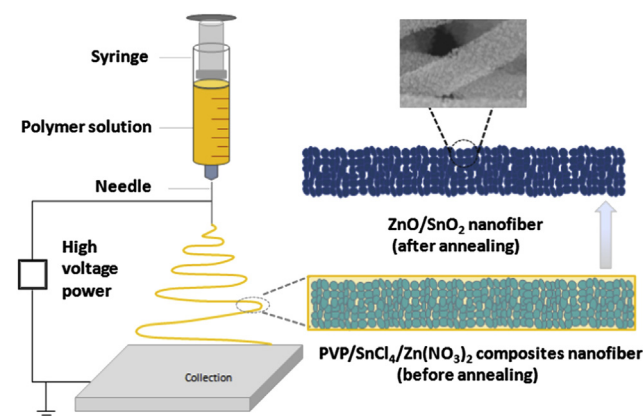
Scheme 1 — Schematic illustration for the formation process of the ZnO/SnO$_2$ nanofibers.
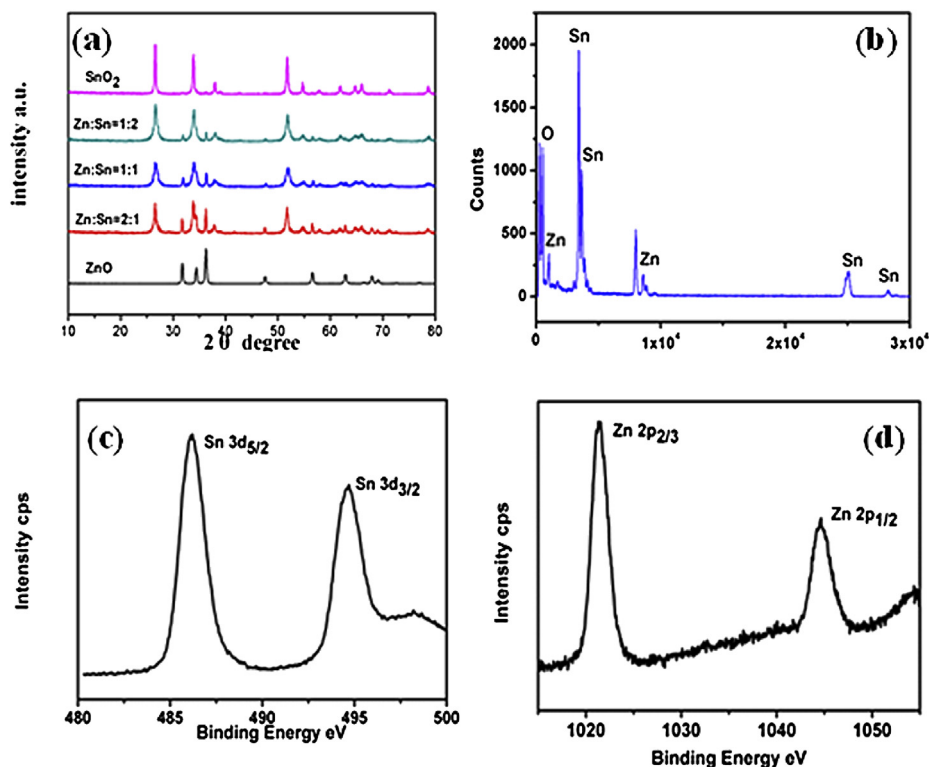
Fig. 1 – (a) XRD patterns of SnO_2 NFs, SnO_2–ZnO-1 NFs, SnO_2–ZnO-2 NFs, SnO_2–ZnO-3 NFs and ZnO NFs; (b) EDX spectrum of SnO_2–ZnO-1 NFs; XPS spectrum of (c) Sn 3d and (d) Zn 2p for the SnO_2–ZnO-1 NFs.

hybrid product is the mixture of SnO_2 and ZnO. When the addition of zinc nitrate gradually increased, the peak intensity of the ZnO NFs accordingly enhances with the feeble of the peaks for SnO_2. The XRD results confirm that the SnO_2–ZnO composites were successfully synthesized via the electrospinning. The typical high-resolution XPS spectra of Sn 3d and Zn 2p for the SnO_2–ZnO-1 NFs are shown in Fig. 1c and d, respectively. Two obvious peaks at 487.6 and 496.1 eV in the Sn 3d spectrum (Fig. 1c) can be assigned to Sn $3d_{5/2}$ and Sn $3d_{3/2}$, respectively [42]. Similarly, the peaks at 1044.5 and 1021.4 eV correspond to the binding energies of Zn $2P_{1/2}$ and Zn $2P_{3/2}$, respectively [43]. It further demonstrates that SnO_2 and ZnO co-exist in the samples.

The morphologies of all the samples were determined by SEM examination. Fig. 2 shows the morphology of the as-prepared $PVP/SnCl_2$ fibers before sintering. It displays a smooth fiber like structure with an average diameter of ~300 nm. Fig. 3 shows the SEM images of the SnO_2 NFs, SnO_2–ZnO-1 NFs, SnO_2–ZnO-2 NFs and SnO_2–ZnO-3 NFs. Fig. 3a, b indicate that the as-prepared SnO_2 NFs well inherit from the unique fibrous. It clearly shows that the SnO_2 NFs are built by the small SnO_2 nanoparticles with the mesoporous structures. The average length of the fibers is about ~2 um, and the diameter is about ~300 nm. After the addition of ZnO, the morphologies of SnO_2–ZnO-1, SnO_2–ZnO-2 and SnO_2–ZnO-3 still maintain the fibrous structure with the
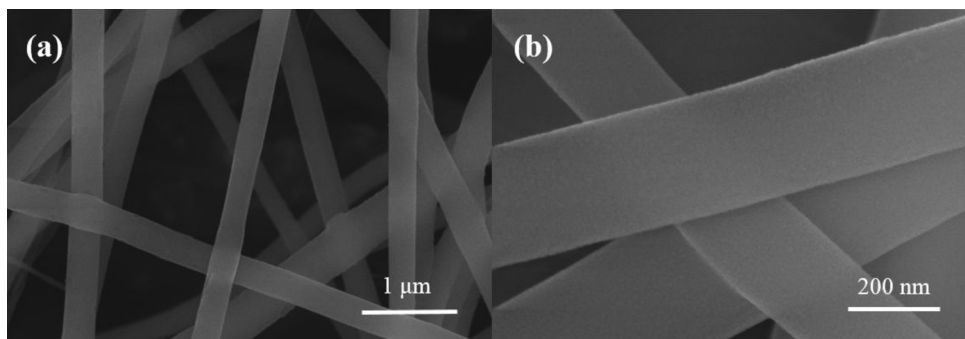

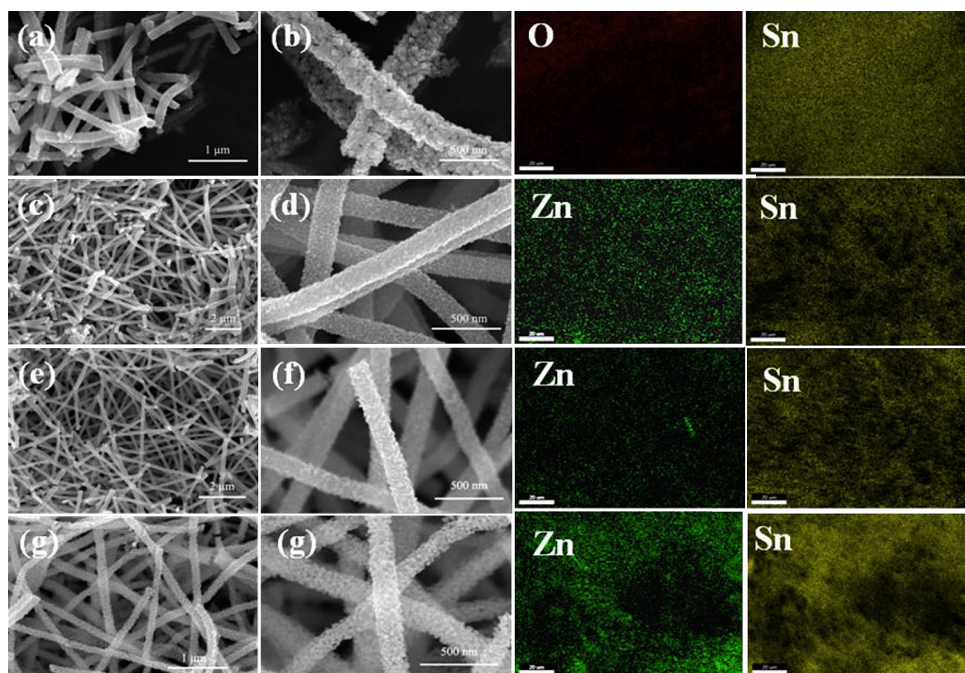**Fig. 2** – Typical SEM images of as prepared $PVP/SnCl_2$ fibers.

Fig. 3 — Typical SEM images of (a, b) SnO$_2$ NFs, (c, d) SnO$_2$—ZnO-1 NFs, (e, f) SnO$_2$—ZnO-2 NFs, (g, h) SnO$_2$—ZnO-3 NFs and the resultant EDX elements mapping.
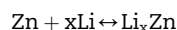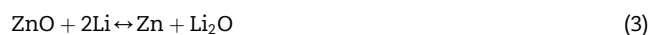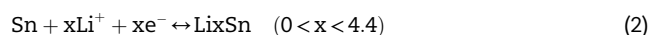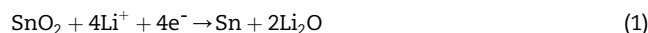
nano-porous. Interestingly, the composite fibers of all three samples become longer and thinner with the smaller particle sizes after ZnO introduction. For example, the average length and diameter of SnO$_2$—ZnO-1 nanofibers is more than ~5um and about ~200 nm with the smoother surface. The addition of ZnO improves the mechanical strength of the nanocomposite fibers, and results in the longer and thinner fibers. However, there are no obvious differences of sizes and morphologies of other two samples with the increasing amount of ZnO. It is considered that the smaller particle sizes will effectively reduce the pulverization and cracking of nanoparticles. The reduced particle size can significantly increase the rate of lithium insertion/extraction, originating from the short distances for lithium-ion transport within the particles [13,44,45].

The elemental mappings of Sn and Zn are compared in Fig. 3 to clarify the distribution of SnO$_2$ and ZnO in the nanocomposites. The images convince the uniform distribution of Sn and Zn elements, which indicates that the SnO$_2$ and ZnO nanoparticles are uniformly distributed along the fibers. Meanwhile, all three samples show the similar trend. The EDX spectrum of SnO$_2$—ZnO-1 in Fig. 1d further confirms the analysis of the elemental mapping in Fig. 3.

As shown in Fig. 4, TEM was performed to elucidate the unique structural feature. Unique fiber-like morphology with the length of more than ~5 μm and diameter of ~200 nm can be clearly observed in Fig. 4a, b, which is in good agreement with the SEM observation. Moreover, the HRTEM images confirm that SnO$_2$—ZnO-1 nanofibers consists of nanoparticles of about ~10 nm in size (Fig. 4c). The clear lattice fringe of 0.340 nm corresponding to (110) of SnO$_2$, and the value of 0.280 nm is related to (110) of ZnO (Fig. 4d). Therefore, the SnO$_2$—ZnO composites with the fiber like morphology were

successfully synthesized in this study via a simple electrospinning technique.

The mechanisms for SnO$_2$—ZnO nanocomposites during the charge/discharge process are as follows:

$$SnO_2 + 4Li^+ + 4e^- \rightarrow Sn + 2Li_2O \tag{1}$$

$$Sn + xLi^+ + xe^- \leftrightarrow LixSn \quad (0 < x < 4.4) \tag{2}$$

$$ZnO + 2Li \leftrightarrow Zn + Li_2O \tag{3}$$

$$Zn + xLi \leftrightarrow Li_xZn$$

The electrochemical performance of all samples as anode materials for LIBs are investigated in detail. Fig. 5 shows the charge/discharge voltage profiles of the SnO$_2$ NFs, SnO$_2$—ZnO-1 NFs, SnO$_2$—ZnO-2 NFs and SnO$_2$—ZnO-3 NFs in the first two cycles in the voltage range of 2—0.01 V at a current density of 100 mA g^{-1}. In the first cycling, the SnO$_2$ NFs delivers a lithium insertion capacity of 1880.7 mAh g^{-1} and a reversible charging capacity of 780 mAh g^{-1}. In the second cycle, the charge and discharge capacities reach 825.1 and 745.1 mA h g^{-1}, respectively, with a coulombic efficiency of over 90%. The large irreversible discharge capacity in the first cycle is due to a side reaction with the electrolyte, which forms Li$_2$O and an SEI film. It can be observed in the first discharge process that an obvious plateau at 0.8 V corresponds to the electrochemical lithium reaction of SnO$_2$ and SEI formation. For the other three profiles, the first discharge (charge) capacities of SnO$_2$—ZnO-1 NFs, SnO$_2$—ZnO-2 NFs and SnO$_2$—ZnO-3 are 1417.4 (599.8), 1408 (774.8) and 1361 (715) mAh g^{-1},
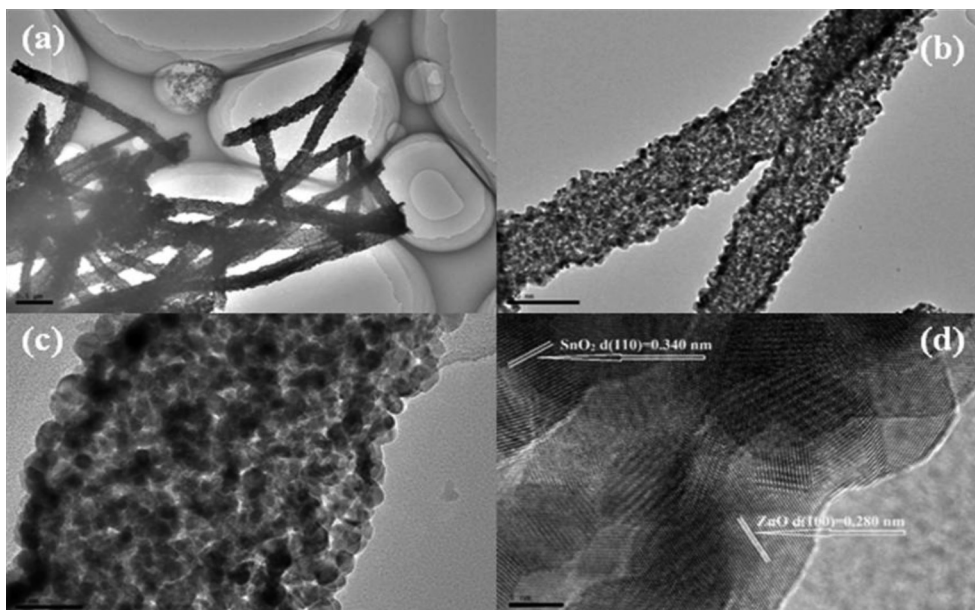
Fig. 4 – (a, b) TEM images and (c, d) HR-TEM images of SnO_2–ZnO-1 NFs.

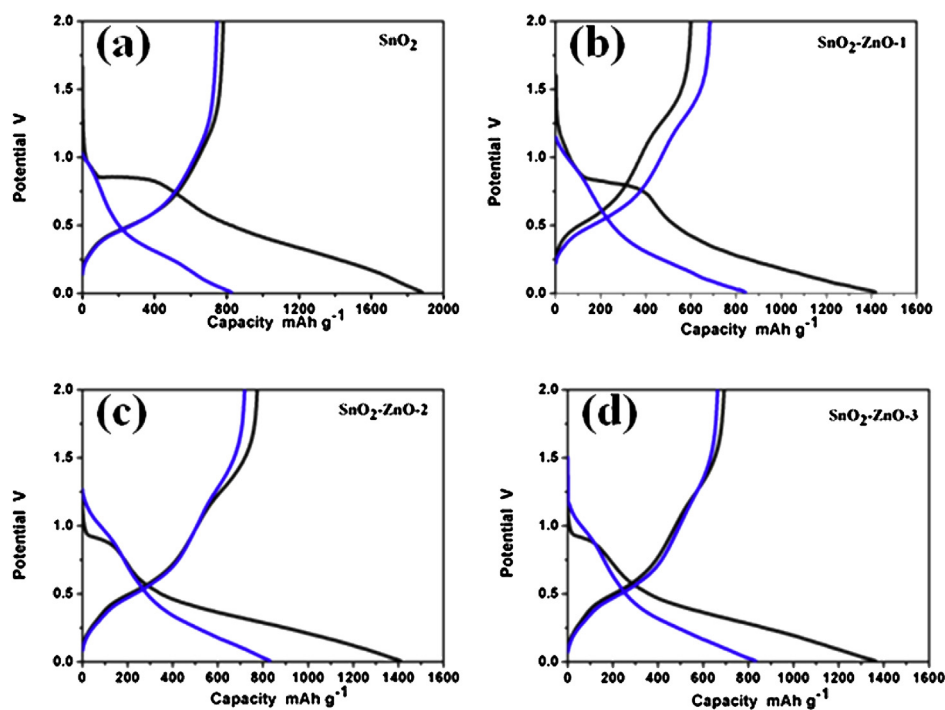**Fig. 5 – Charge/discharge voltage profiles of (a) SnO_2 NFs, (b) SnO_2–ZnO-1 NFs, (c) SnO_2–ZnO-2 NFs and (d) SnO_2–ZnO-3 NFs for the first two cycles.**

respectively. One can see that the initial capacities of the nanocomposites decrease with the increased amount of ZnO due to its low theoretical capacity.

The cyclability comparison of SnO_2 NFs, SnO_2–ZnO-1 NFs, SnO_2–ZnO-2 NFs, SnO_2–ZnO-3 NFs and ZnO was carried out, which is shown in Fig. 6a. After 5 cycles, the reversible capacity of ZnO fades rapidly into 60 mAh g^{-1}, indicating the low

electrochemical activity. For SnO_2 NFs, the retained reversible capacity is near 200 mA h g^{-1} after 20 cycles originating from the large volume change of Sn and the poor kinetics of the electrochemical conversion reaction. After the addition of ZnO, the reversible capacity of SnO_2–ZnO-1 NFs, SnO_2–ZnO-2 NFs and SnO_2–ZnO-3 are 430.6, 302.1, and 248.5 mA h g^{-1}, respectively. Clearly, the SnO_2–ZnO-1 NFs indicates the best
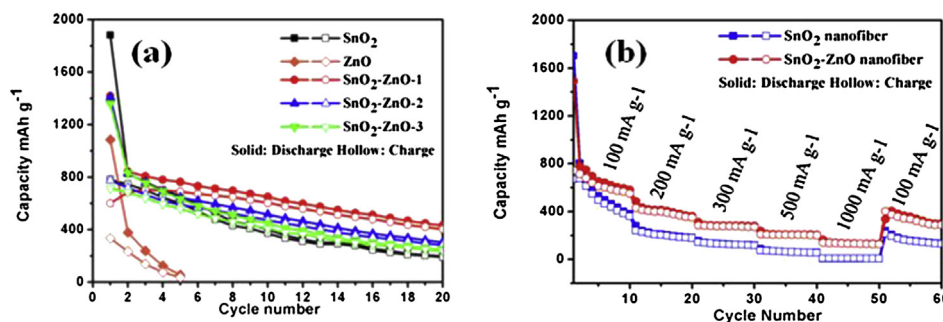
Fig. 6 – (a) The comparison of cycling performance of the SnO$_2$ NFs, SnO$_2$–ZnO-1 NFs, SnO$_2$–ZnO-2 NFs, SnO$_2$–ZnO-3 NFs and ZnO at a current density of 100 mA g^{-1} in a voltage range of 0.01–2.0 V; (b) Rate capability of the SnO$_2$ NFs and SnO$_2$–ZnO-1 NFs in a voltage range of 0.01–2.0 V.

improvement. Fig. 6b show the comparison of the rate performance between SnO$_2$ NFs and SnO$_2$–ZnO-1 NFs. At different current densities of 200, 300, 500 and 1000 mA g^{-1}, the discharge capacities of SnO$_2$–ZnO-1 NFs are 350.5, 270.6, 200.1 and 125.7 mAh g^{-1}. When the current densities back to 100 mA g^{-1}, the capacity climbs up to 288.9 mAh g^{-1}. Clearly, the SnO$_2$–ZnO-1 NFs deliver the better rate performances than the pristine SnO$_2$ NFs, which demonstrate the advantages of the hybrid nanoscomposites in LIBs. The performance improvement is due that the two types of metal elements with different expansion coefficient have the synergistic effect. ZnO functions as soft matrix buffering the volume expansion/shrinkage during alloying/de-alloying. However, with the further increased content of ZnO, the electrochemical performances of the hybrid nanocomposites show the opposite trend, which result from the low electrochemical activity of ZnO.

Conclusions

The SnO$_2$–ZnO nanofibers were successfully synthesized by a simple electrospinning method. It has been found that SnO$_2$–ZnO composite is a promising anode material for LIBs, as it exhibits an enhanced lithium storage capacity, cycling performance and rate properties than the pristine SnO$_2$ NFs and ZnO NFs. The performance improvement can be ascribed to the introduction of ZnO, which act as buffer matrix for the huge volume change. Meanwhile, the influence of the content of ZnO in the composites has been discussed. Thus, as-prepared SnO$_2$–ZnO NFs shows its great potentials for the applications in LIBs.

Acknowledgments

REFERENCES

[1] Scrosati B, Hassoun J, Sun Y-K. Lithium-ion batteries. A look into the future. Energy Environ Sci 2011;4:3287.
[2] Poizot P, Laruelle S, Grugeon S, Dupont L, Tarascon J. Nano-sized transition-metal oxides as negative-electrode materials for lithium-ion batteries. Nature 2000;407:496–9.
[3] Tarascon J-M, Armand M. Issues and challenges facing rechargeable lithium batteries. Nature 2001;414:359–67.
[4] Armand M, Tarascon J-M. Building better batteries. Nature 2008;451:652–7.
[5] Huang Y, Huang XL, Lian JS, Xu D, Wang LM, Zhang XB. Self-assembly of ultrathin porous NiO nanosheets/graphene hierarchical structure for high-capacity and high-rate lithium storage. J Mater Chem 2012;22:2844–7.
[6] Huang XL, Wang RZ, Xu D, Wang ZL, Wang HG, Xu JJ, et al. Homogeneous CoO on graphene for binder-free and ultralong-life lithium ion batteries. Adv Funct Mater 2013;23:4274–353.
[7] Wang HG, Ma DL, Huang XL, Huang Y, Zhang XB. General and controllable synthesis strategy of metal Oxide/TiO$_2$ hierarchical heterostructures with improved lithium-ion battery performance. Sci Rep 2012;2:701.
[8] Wang ZL, Xu D, Wang HG, Wu Z, Zhang XB. In situ fabrication of porous graphene electrodes for high-performance energy storage. ACS Nano 2013;7:2422–30.
[9] Huang XL, Zhao X, Wang ZL, Wang LM, Zhang XB. Facile and controllable one-pot synthesis of an ordered nanostructure of Co(OH)$_2$ nanosheets and their modification byoxidation for high-performance lithium-ion batteries. J Mater Chem 2012;22:3764–9.
[10] Huang XL, Chai J, Jiang T, Wei YJ, Chen G, Liu WQ, et al. Self-assembled large-area Co(OH)$_2$ nanosheets/ionic liquid modified graphene heterostructures toward enhanced energy storage. J Mater Chem 2012;22:3404–10.
[11] Xie J, Yang XG, Zhou S, Wang DW. Comparing one-and two-dimensional heteronanostructures as silicon-based lithium ion battery anode materials. ACS Nano 2011;5:9225–31.
[12] Arico AS, Bruce PG, Scrosati B, Tarascon JM, Schalkwijk WV. Nanostructured materials for advanced energy conversion and storage devices. Nat Mater 2005;4:366–77.
[13] Zhao Y, Li XF, Yan B, Li DJ, Lawes S, Sun XL. Significant impact of 2D graphene nanosheets on large volume change

tin-based anodes in lithium-ion batteries: a review. J Power Sources 2015;274:869–84.

[14] Zhao Y, Huang Y, Sun X, Huang HJ, Wang K, Zong M, et al. Hollow Zn_2SnO_4 boxes wrapped with flexible graphene as anode materials for lithium batteries. Electrochim Acta 2014;120:128–32.

[15] Zhao Y, Huang Y, Wang QF, Wang K, Zong M, Wang L, et al. Preparation of hollow Zn_2SnO_4 boxes for advanced lithium-ion batteries. RSC Adv 2013;3:14480.

[16] Wang QF, Huang Y, Miao J, Zhao Y, Wang Y. Synthesis and electrochemical characterizations of Ce doped SnS_2 anode materials for rechargeable lithium ion batteries. Electrochimica Acta 2013;93:120–30.

[17] Wang DN, Yang JL, Li XF, Geng DS, Li RY, Cai M, et al. Layer by layer assembly of sandwiched graphene/SnO_2 nanorod/carbon nanostructures with ultrahigh lithium ion storage properties. Energy Environ Sci 2013;6:2900.

[18] Goriparti S, Miele E, Angelis FD, Fabrizio ED, Zaccaria RP, Capiglia C. Review on recent progress of nanostructured anode materials for Li-ion batteries. J Power Sources 2014;257:421–43.

[19] Chen JS, Lou XW. SnO_2-based nanomaterials: synthesis and application in lithium-ion batteries. Small 2013;9:1877–93.

[20] Li X, Meng X, Liu J, Geng D, Zhang Y, Banis M, et al. Tin oxide with controlled morphology and crystallinity by atomic layer deposition onto graphene nanosheets for enhanced lithium storage. Adv Funct Mater 2012;22:1647–54.

[21] Paek SM, Yoo EJ, Honma I. Enhanced cyclic performance and lithium storage capacity of SnO_2/Graphene nanoporous electrodes with three-dimensionally delaminated flexible structure. Nano Lett 2009;9:72–5.

[22] Zhu JJ, Lu ZH, Aruna ST, Aurbach D, Gedanken A. Sonochemical synthesis of SnO_2 nanoparticles and their preliminary study as Li insertion electrodes. Chem Mater 2000;12:2557–66.

[23] Park MS, Wang GX, Kang YM, Wexler D, Dou SX, Liu HK. Preparation and electrochemical properties of SnO_2 nanowires for application in lithium-ion batteries. Angew Chem 2007;119:764–7.

[24] Ying Z, Wan Q, Cao H, Song ZT, Feng SL. Characterization of SnO_2 nanowires as an anode material for Li-ion batteries. Appl Phys Lett 2005;87:113108–113108-3.

[25] Ye JF, Zhang HJ, Yang R, Li XG, Qi LM. Morphology-controlled synthesis of SnO_2 nanotubes by using 1D silica mesostructures as sacrificial templates and their applications in lithium-ion batteries. Small 2010;6:296–306.

[26] Wang Y, Zeng HC, Lee JY. Highly reversible lithium storage in porous SnO_2 nanotubes with coaxially grown carbon nanotube overlayers. Adv Mater 2006;18:645–9.

[27] Wang C, Zhou Y, Ge MY, Xu XB, Zhang ZL, Jiang JZ. Large-scale synthesis of SnO_2 nanosheets with high lithium storage capacity. J Am Chem Soc 2010;132:46–7.

[28] Lou XW, Wang Y, Yuan CL, Lee JY, Archer LA. Template-free synthesis of SnO_2 hollow nanostructures with high lithium storage capacity. Adv Mater 2006;18:2325–9.

[29] Cakan RD, Hu YS, Antonietti M, Maier J, Titirici MM. Facile one-pot synthesis of mesoporous SnO_2 microspheres via

[30] Wang ZY, Luan DY, Boey FYC, Lou XW. Fast formation of SnO_2 nanoboxes with enhanced lithium storage capability. J Am Chem Soc 2011;133:4738–41.

[31] Feng N, Qiao L, Hu DK, Sun XL, Wang P, He DY. Synthesis, characterization, and lithium-storage of ZnO–SnO_2 hierarchical architectures. RSC Adv 2013;3:7758–64.

[32] Kim DW, Hwang IS, Kwon SJ, Kang HY, Park KS, Choi YJ, et al. Highly conductive coaxial SnO_2-In_2O_3 heterostructured nanowires for Li ion battery electrodes. Nano Lett 2007;7:3041–5.

[33] Li YF, Hu YJ, Jiang H, Hou XY, Li CZ. Construction of core–shell Fe_2O_3@SnO_2 nanohybrids for gas sensors by a simple flame-assisted spray process. CrystEngComm 2013;15:6715.

[34] Lin YM, Nagarale RK, Klavetter KC, Heller A, Mullins CB. SnO_2 and TiO_2-supported-SnO_2 lithium battery anodes with improved electrochemical performance. J Mater Chem 2012;22:11134.

[35] Li D, Xia YN. Electrospinning of nanofibers: reinventing the wheel? Adv Mater 2004;16:1151–70.

[36] Xia X, Wang X, Zhou HM, Niu X, Xue LG, Zhang XW, et al. The effects of electrospinning parameters on coaxial Sn/C nanofibers: morphology and lithium storage performance. Electrochimica Acta 2014;121:345–51.

[37] Luo W, Hu XL, Sun YM, Huang YH. Electrospun porous $ZnCo_2O_4$ nanotubes as a high-performance anode material for lithium-ion batteries. J Mater Chem 2012;22:8916.

[38] Yu Y, Gu L, Wang CL, Dhanabalan A, Aken PA, Maier J. Encapsulation of Sn@carbon nanoparticles in bamboo-like hollow carbon nanofibers as an anode material in lithium-based batteries. Angew Chem Int Ed 2009;48:6485–9.

[39] Li LM, Yin XM, Liu S, Wang YG, Chen LB, Wang TH. Electrospun porous SnO_2 nanotubes as high capacity anode materials for lithium ion batteries. Electrochem Commun 2010;12:1383–6.

[40] Zhang ZY, Shao CL, Li XH, Zhang L, Xue HM, Wang CH, et al. Electrospun nanofibers of ZnO–SnO_2 heterojunction with high photocatalytic activity. J Phys Chem C 2010;114:7920–5.

[41] Choi SW, Park JY, Kim SS. Synthesis of SnO_2–ZnO core–shell nanofibers via a novel two-step process and their gas sensing properties. Nanotechnology 2009;20:465603.

[42] Guo Q, Qin X. Flower-like SnO_2 nanoparticles grown on graphene as anode materials for lithium-ion batteries. J Solid State Electrochem 2014;18:1031–9.

[43] Wan Q, Yu K, Wang TH, Lin CL. Low-field electron emission from tetrapod-like ZnO nanostructures synthesized by rapid evaporation. Appl Phys Lett 2003;83:2253.

[44] Chen S, Wang Y, Ahn H, Wang G. Microwave hydrothermal synthesis of high performance tin–graphene nanocomposites for lithium ion batteries. J Power Sources 2012;216:22–7.

[45] Kim C, Noh M, Choi M, Cho J, Park B. Critical size of a nano SnO_2 electrode for Li-secondary battery. Chem Mater 2005;17:3297–301.